III-1

Accelerators and Instruments

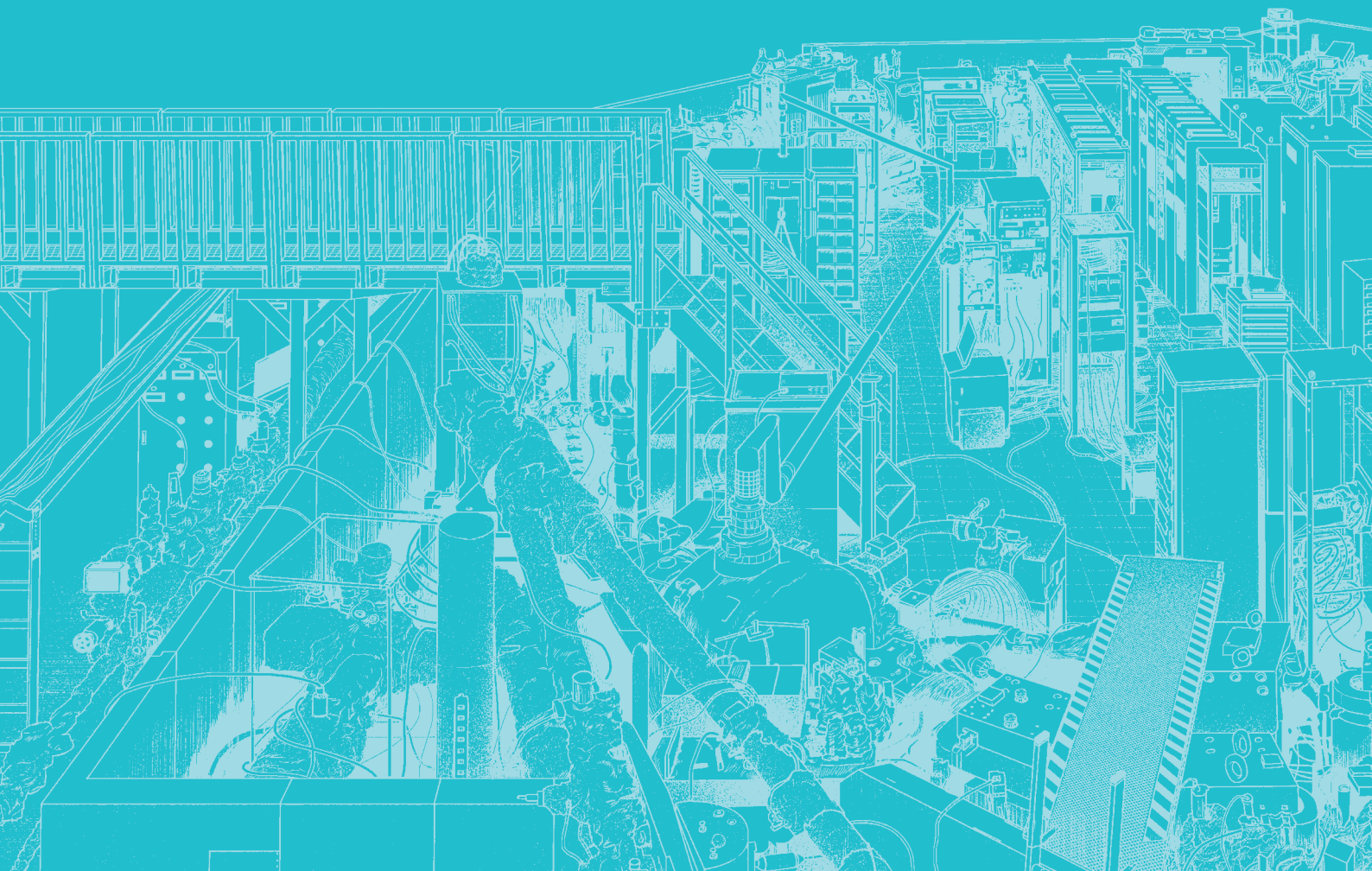

High light

BL5U

Spin-Polarized Band Mapping in Au(111) Surface States

J. Okabayashi[1] and K. Tanaka[2]

[1]*Research Center for Spectrochemistry, The University of Tokyo, Bunkyo-ku, Tokyo 113-0033, Japan*

[2]*UVSOR Synchrotron Facility, Institute for Molecular Science, Okazaki 444-8585*

Spintronics is a rapidly emerging field of science and technology that will most likely have a significant impact on the future of all aspects of electronics. Understanding magnetism of surfaces, interfaces, and nanostructures is greatly important for realizing the spintronics which aims to control and use the function of spin as well as the charge of electrons. Spin- and angle-resolved photoemission spectroscopy (spin-resolved ARPES) is one of the most powerful experimental techniques to investigate the magnetic properties of such materials, where one can know the "complete" information of the electronic states of materials, that is, energy, momentum, and spin direction. Recent development of high energy and angle-resolved photoelectron analyzer as well as the contemporary light sources makes it possible for the photoemission spectroscopy to investigate not only band structures but also many body interactions of electrons in solids. However, appending the spin resolution to photoemission spectroscopy is quite difficult because of an extremely low efficiency (10^{-4}) of Mott-type spin detections.

Recently, very low-energy electron diffraction (VLEED-type) spin detector with 100 times higher efficiency than that of conventional Mott-type has been developed and spin-resolved ARPES has been started to be realized [1-3]. So far, most of the spin-resolved ARPES systems are using the single-channel detector and efficiency is still a problem. We have developed high-efficient spin-resolved ARPES system with multi-channel detection (we call "image-spin" detection) to achieve the 100 times better efficiency and the 10 times better momentum resolution than the current spin-resolved ARPES system, which can be a breakthrough in this research field.

Figure 1 shows the ARPES and spin-resolved ARPES images in Au(111) surface states. Rashba-type spin-split surface states are clearly detected with the Fermi surface mapping. We succeeded in obtaining a spin-resolved signal on the Au(111) surface as shown in Fig. 1(c). According to rough estimates, the efficiency of spin-resolved ARPES was 100 times higher than that of the single-channel detection systems currently used in the world. However, the spin-resolved ARPES bands were broad compared to the normal ARPES ones shown in Fig. 1(b), meaning that the momentum resolution was not so good. To overcome these problems, we have introduced a new "spin manipulator" that can change the spin direction of the passing electrons in any direction. The installation of the spin manipulator and optimization of the spin target deposition conditions have greatly improved the spin-resolved images, and we were able to obtain spin-resolved images with momentum resolution comparable to that of normal ARPES, as shown in Fig. 1(d). We are currently optimizing the lens parameters of the spin manipulator to obtain spin information in the remaining two axial directions.

[1] C. Bigi *et al*., J. Synchrotron Rad. **24** (2017) 750.
[2] T. Okuda, J. Phys.: Condens. Matter **29** (2017) 483001.
[3] F. Ji *et al.,* Phys. Rev. Lett. **116** (2016) 177601.

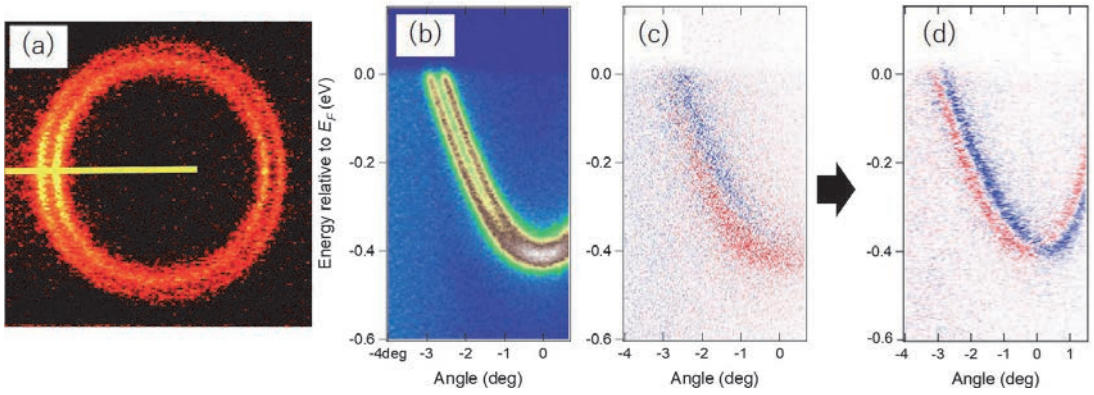

Fig. 1. a) Fermi surface of Rashba spin splitting in Au(111) surface states and (b) image plot of normal ARPES along the yellow bar in (a). Spin-resolved ARPES data showing the spin polarization (blue–red scale) with the previous experimental setup (c) and the current setup (d).

BL1U

Improvement of Accuracy of Non-Destructive Nuclide Assay by Transmission NRF Method

T. Shizuma[1,2], M. Omer[2], R. Hajima[1], M. Koizumi[2], H. Zen[3], H. Ohgaki[3] and Y. Taira[4]

[1]*National Institutes for Quantum Science and Technology, Kizugawa 619-0215, Japan*

[2]*Japan Atomic Energy Agency, Tokai 319-1195, Japan*

[3]*Institute of Advanced energy, Kyoto University, Uji 611-0011, Japan*

[4]*UVSOR Synchrotron Facility, Institute for Molecular Science, Okazaki 444-8585, Japan*

Nuclear resonance fluorescence (NRF) is a process in which atomic nuclei absorb and emit γ rays. Because the emitted γ rays have energies specific to each nuclide, it is possible to identify the nuclide by measuring the energy of emitted NRF γ rays. Furthermore, because a γ-ray beam at MeV energy range that has high penetrating power is used in NRF experiments, non-destructive measurement is possible even when the sample is placed in a heavy shield. In transmission NRF, a γ-ray beam that passes through an absorption target is irradiated to another target (called witness plate, WP) which consists of the same nuclide as the absorption target, and NRF γ rays emitted from the WP target are measured. Transmission NRF is favorable over scattering NRF measurements because the effect of background radiation can be reduced [1].

The absorption amount of γ rays in transmission NRF depends on the temperature of absorption and WP targets due to the Doppler broadening of resonant width. Therefore, the temperature of the absorption or WP targets may affect the time and sensitivity of the measurement. To study the temperature dependence of the self-absorption, we irradiated ^{206}Pb samples at room or LN_2 temperatures with a laser Compton scattering (LCS) γ-ray beam. LCS γ rays with maximum energy of 5.54 MeV were produced from the collision of 746-MeV electrons with laser photons with a wavelength of 1.895 μm. A lead collimator with 20-cm thickness and 3-mm aperture size was used to confine the LCS γ-rays to the energy width to approximately 8% (FWHM). Two high-purity Ge detectors, located horizontally at a scattering angle 90° with respect to the incident γ-ray direction, were used to detect NRF γ-rays, as shown in Fig. 1.

Figure 2 shows typical spectra measured with (black) and without (red) the absorption target at room temperature. NRF peaks of ^{206}Pb [2] are observed at 4971, 5037, 5127, 5377, 5459, 5470, and 5524 keV. The spectrum with the absorption target is corrected for atomic absorption, therefore showing only nuclear resonant absorption (so called self-absorption) effect. The upper spectrum (blue) represents the difference of the counts obtained with and without the absorption target which visualizes the self-absorption yields by negative counts. The largest self-absorption occurs in the resonance at 5037 keV which has the integrated cross section of 1150 eV b. From the present measurements, self-absorption amounts consistent with theory are obtained.

This work is in part a contribution of JAEA to IAEA coordinated research program, J02015.

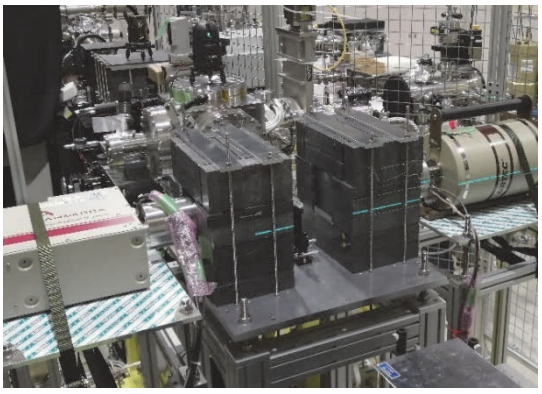

Fig. 1. Photo of the experimental setup used for the transmission NRF measurements.

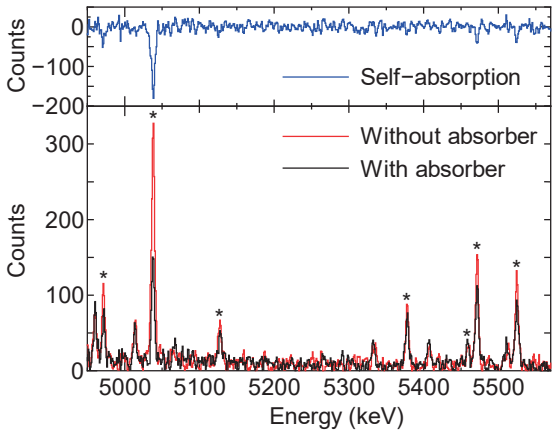

Fig. 2. Typical γ-ray spectra obtained in transmission NRF experiments. In the lower panel, the red (black) spectrum corresponds to the measurement without (with) the absorption target at room temperature. Asterisks indicate NRF peaks of ^{206}Pb. The upper spectrum (blue) represents the difference of the spectra measured with and without absorption target, indicating the amount of self-absorption.

[1] C.T. Angell *et al.*, Nucl. Instrum. Methods Phys. Res., Sect. B **347** (2006) 11.

[2] T. Shizuma *et al.*, Phys. Rev. C: Nucl. Phys. **98** (2018) 064317.

BL1U

Gamma-ray Polarization Measurement with GAGG Pixel Detectors

K. Shimazoe [1], R. Sato[1], M. Uenomachi[2] and Y. Taira[3]
[1]*Graduate School of Engineering, The University of Tokyo, Tokyo 113-8656, Japan*
[2]*Space Unit, Kyoto University, Kyoto 606-8502, Japan*
[3]*UVSOR Synchrotron Facility, Institute for Molecular Science, Okazaki 444-8585, Japan*

Polarization measurement of gamma-rays emitted from nuclei can give a useful information in nuclear physics and medical application. For example, recently the use of quantum entanglement in polarization of two gamma-rays emitted from positron-electron annihilation is proposed and it can contribute the image quality improvement in PET (Positron Emission Tomography) [1]. Generally, the measurement of polarization in gamma-rays can be conducted through the detection of Compton scattering angle influenced by polarization angle. Our group have been developing a Compton-PET imaging system[2] for visualizing multi-nuclides simultaneously in the nuclear medical imaging framework.

In this study, we have designed a multi-channel gamma-ray pixel detector system with modules composed of 8 × 8 GAGG scintillators coupled to 8 × 8 SiPM array. 8 modules with 512 pixels are used to detect the scattered gamma-ray for recording the scattering angle of linearly polarized, circularly polarized and non-polarized gamma-rays. All the pixels' signals are readout with individually coupled dynamic time-over-threshold circuit [3] to record its energy, time and position for reconstructing the scattering angle. Figure 1 shows the experimental setup with 8 modules. All the pixel timing is recorded with a synchronized digital time-to-digital converter system with FPGA based DAQ [4].

6.6 MeV polarized gamma-rays generated in UVSOR are irradiated to scatterer and Compton scattered events are extracted from the recorded list-mode data. Fig. 2 shows the coincidence time histogram between scatterer and absorber.

Using the coincidence events, the angle of Compton scattering was calculated and plotted calibrated by the non-polarized gamma-rays. Figure 3 shows the case of 135-degree polarization.

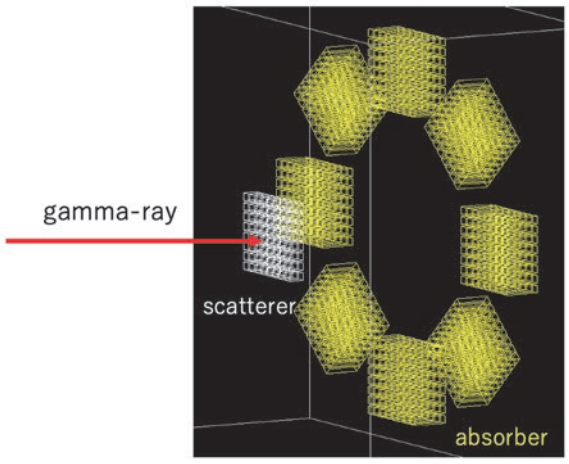

Fig. 1. Polarization detection setup with 512 channel GAGG-SiPM pixel detectors.

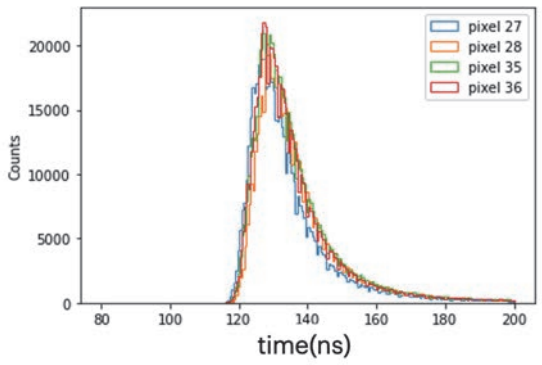

Fig. 2. Coincidence time histogram between scatterer and absorber for measuring Compton scattering events.

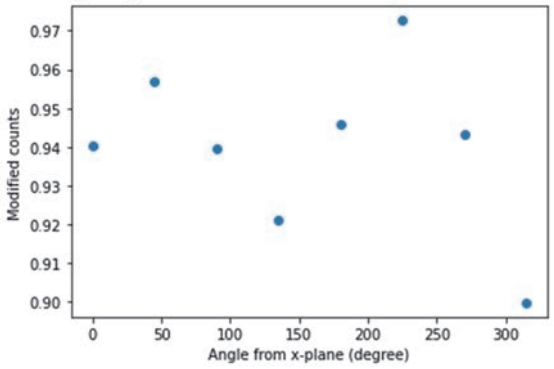

Fig. 3. Measured counts in 135-degree polarization. Sine curve is successfully observed.

[1] Kim, Donghwan *et al*., J. Instrum. **18.07** (2023) P07007.
[2] Uenomachi, Mizuki *et al*., Sci. Rep. **11.1** (2021) 17993.
[3] Shimazoe, Kenji, *et al*. IEEE Trans. Nucl. Sci. **59.6** (2021) 3213.
[4] Sato, S., Uenomachi, M. and Shimazoe, K. IEEE Trans. Nucl. Sci. **68** (2021) 1801.

BL1U

Generation of F-LCS Gamma-rays for Isotope Selective Imaging Study in UVOSR BL1U

H. Ohgaki[1], S. Tanizaki[1], H. Zen[1], T. Kii[1], T. Hayakawa[2,3] and T. Shizuma[2]
[1]*Institute of Advanced Energy, Kyoto University, Kyoto 611-0011, Japan*
[2]*Kansai Photon Science Institute, National Institutes for Quantum Science and Technology, Kizugawa, Kyoto 619-0215, Japan*
[3]*Institute of Laser Engineering, Osaka University, Suita 565-0871, Japan*

Flat Laser Compton Scattering Gamma-ray beam (F-LCS), which has a flat distribution in the energy spectrum and the spatial distribution with a few mm diameter beam size, has been developed to study an isotope selective CT Imaging application in the beamline BL1U in UVSOR. By using a circular motion of the electron beam which is excited by a helical undulator installed in a storage ring, and collision with an intense laser beam, an F-LCS beam can be generated.

A POP experiment was carried out at the BL1U in UVSOR in 2022 machine time and we obtained larger K-value of undulator, the broader energy bandwidth of the LCS was observed as predicted by EGS5 simulation [1,2].

In 2023, we tried to obtain a multi-isotopes imaging by using F-LCS beam generated in BL1U to excite NRF levels of $^{206, 207, 208}$Pb as the target isotopes. Three enriched isotope targets of 8 mmϕ rods were prepared for the imaging sample, and three enriched isotope witness targets were placed behind the imaging sample, as shown in Fig.1.Two large high-purity Ge detectors recorded NRF gamma rays from the witness targets. A normal LCS beam (undulator K-value=0) and F-LCS (K=0.2) were generated by using a Tm-fiber laser system (TLR-50-AC-Y14, IPG Laser GmbH) with an output power of around 30 W colliding with the electron beam of 746 MeV whose beam current was 200 mA. Due to the available gamma ray yields and the machine time, the scanning step of 7 mm was chosen to measure the F-LCS irradiation and 14 mm to the LCS irradiation. Figure 2 shows the NRF spectra with LCS (black line) and F-LCS (red line). Using F-LCS, the 5037 keV peak from ^{206}Pb was clearly observed because of broader energy spectrum of the F-LCS beam.

Figures 3 show the results of NRF imaging of ^{208}Pb (a) and ^{207}Pb (b) with the LCS beam (black lines) and F-LCS beam (red lines). As the results, we obtained multi-isotopes NRF imaging with LCS and F-LCS beams. However, we could not obtain the NRF imaging of ^{206}Pb even with the F-LCS beam.

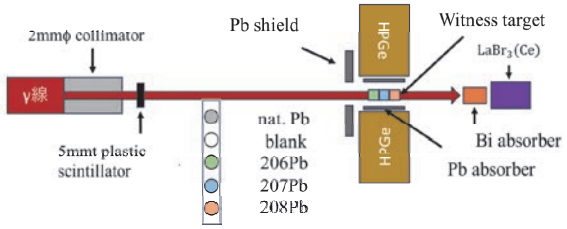

Fig. 1. Schematic drawing of the experimental set-up.

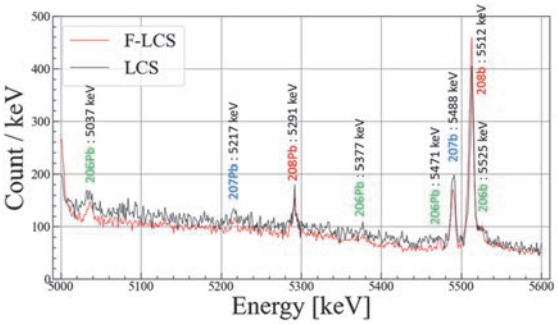

Fig. 2. LCS gamma-ray energy distribution in the vertical axis with the undulator K-value of K=0.2.

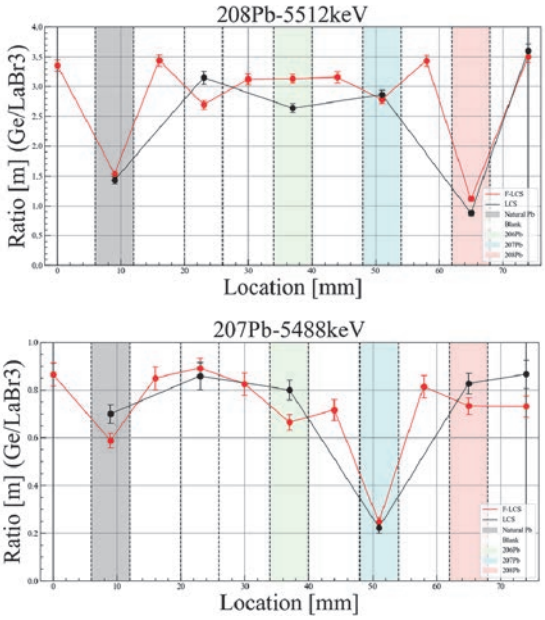

Fig. 3. Upper (a) Measured 1D NRF imaging of 208Pb and lower (b) 207Pb. Black lines shows the result with the LCS beam and Red lines shows the result with the F-LCS beam.

[1] H. Ohgaki *et al*., UVSOR Activity Report **50** (2023) 40.
[2] H. Ohgaki *et al*., Phys. Rev. Accel. Beams **26** (2023) 093402.

BL1U

Experimental Study on Radiation from Single Electron

Y. Asai[1], H. Miyauchi[2, 3], M. Shimada[2, 3] and M. Katoh[2, 4]
[1]*Graduate School of Advanced Science and Engineering, Hiroshima University, Higashi-Hiroshima 739-8526, Japan*
[2]*Hiroshima Synchrotron Radiation Center, Hiroshima University, Higashi-Hiroshima 739-0046*
[3]*High Energy Accelerator Research Organization (KEK), Tsukuba 305-0801, Japan*
[4]*UVSOR Synchrotron Facility, Institute for Molecular Science, Okazaki 444-8585, Japan*

We have demonstrated experimentally at UVSOR BL1U that undulator radiation has characteristic spatiotemporal structures. For example, helical undulator radiation possesses spiral phase structures [1] and tandem undulator (two undulators in series) double-pulse waveforms [2]. Undulator radiation from synchrotron light sources is considered as an incoherent mixture of wave packets emitted from each individual electron, in contrast to the coherent radiation emitted from free electron lasers. There arises a question whether radiation from a single electron has those spatiotemporal structures that we have shown for the radiation from an ensemble of huge number of electrons, typically $10^{11\sim12}$[1, 2].

To realize an experimental study on the radiation from a single electron, the simplest approach is accumulating only one electron in synchrotron. Such single electron storage has been realized in a few synchrotrons, aiming to studies on electron dynamics [3, 4. 5], radiation [6, 7] and primary standard [8]. We have started single electron storage experiments at UVSOR since 2021 with the aim of conducting fundamental research on electromagnetic radiation from a single electron. The method is basically same as the previous studies. We inject one pulse of electron beam from the booster synchrotron to the storage ring. The accumulated beam current is typically much smaller than 1mA. Then, we insert the beam scraper to reduce the electron beam intensity, as observing the undulator radiation intensity tuned at the wavelength of 355 nm at the beamline BL1U by using a photomultiplier tube. We succeeded in observing a step-function-like intensity change under a small number of electron storage conditions with a good SN ratio and in confirming the single electron storage [9, 10]. In 2022, we continue improving the method of observing the accumulation state of single electron and, then, attempted to observe undulator radiation from single electron [11, 12].

We tried to observe radiation emitted from a tandem undulator, which consists of two undulators arranged in series. It is known that the synchrotron radiation from the tandem undulator shows a finely modulated spectrum with the envelope of that from one undulator [13]. This modulation is the result of the spectral interference between the radiation from two undulators.

The number of photons emitted during single passage of an electron in the undulator is much less than unity, which is in the same order of the fine structure constant. Therefore, under the single electron storage, the probability that the electron emits more than two photons is negligible. The aim of this experiment is to show that, even in the condition that the single electron radiate only one photon in the tandem undulator, the spectrum shows the modulation or not. This is similar to Young's interference experiment in the photon counting regime but in the time domain.

We constructed a simple measurement system consisting of a grating and a cooled CCD camera. Because the photon beam intensity was very low, we had to make the exposure time as long as 1 hour. To get a clear data, the background subtraction should be made very carefully. After trial and error, we found that the background taken for same exposure time should be used. This gave very clear data which shows that the spectrum of the tandem undulator radiation emitted by single electron shows clear modulation as that emitted from ensemble of electrons. The result has been reported elsewhere [14, 15, 16], and will be published in the nearest future.

[1] M. Katoh *et al*., Sci. Rep. **7** (2017) 6130.
[2] T. Fuji *et al*., Optica **10** (2023) 302.
[3] I.V. Pinayev *et al*., Nucl. Instrum. Methods Phys. Res., Sect. A **375** (1996) 71.
[4] A. N. Aleshaev *et al*., Nucl. Instrum. Methods Phys. Res., Sect. A **359** (1995) 80.
[5] A. Romanov *et al.,* JINST **16** (2021) P12009.
[6] I.V. Pinayev *et al*., Nucl. Instrum. Methods Phys. Res., Sect. A **341** (1994) 17.
[7] I. Lobach *et al*., JINST **17** (2022) P02014.
[8] R. Klein *et al*., Phys. Rev. Accel. Beams **11** (2008) 110701.
[9] R. Shinomiya *et al*., UVSOR Activity Report **49** (2022) 40.
[10] R. Shinomiya *et al*., presented at JSR2022, 9PS01S (Jan., 2022).
[11] Y. Asai *et al*., presented at JSR2023, 1F03S (Jan., 2023).
[12] Y. Asai *et al*., UVSOR Activity Report **49** (2023) 42.
[13] M. Billardon *et al*., J. Phys. Collques **44** (1983) 29.
[14] Y. Asai *et al*., presented at PASJ2023, WEP26 (Aug. 2023).
[15] Y. Asai *et al*., presented at 2023 Annual meeting of JPS, 19aRD11, 3 (Sep., 2023).
[16] Y. Asai *et al*., presented at 2023 HiSOR Symp., P02S (Mar., 2023).

BL1U

Frequency-Domain Determination of Time Delay between Two Light Wave Packets Generated by a Tandem Undulator

Y. Hikosaka[1], T. Kaneyasu[2,3], S. Wada[4], H. Kohguchi[4], H. Ota[3], E. Nakamura[3], H. Iwayama[3,5], M. Fujimoto[6], M. Hosaka[7] and M. Katoh[3,5,8]

[1]*Institute of Liberal Arts and Sciences, University of Toyama, Toyama 930-0194, Japan*
[2]*SAGA Light Source, Tosu 841-0005, Japan*
[3]*Institute for Molecular Science, Okazaki 444-8585, Japan*
[4]*Graduate School of Advanced Science and Engineering, Hiroshima University, Higashi-Hiroshima 739-8526, Japan*
[5]*Sokendai (The Graduate University for Advanced Studies), Okazaki 444-8585, Japan*
[6]*Synchrotron Radiation Research Center, Nagoya University, Nagoya 464-8603, Japan*
[7]*National Synchrotron Radiation Laboratory, University of Science and Technology of China, Hefei 230029, China*
[8]*Hiroshima Synchrotron Radiation Center, Hiroshima University, Higashi-Hiroshima 739-0046, Japan*

Our recent works [1-5] have demonstrated that time-domain interferometry of atoms, which was thought to be possible only with lasers with excellent temporal coherence, can be realized with synchrotron radiation generated by a tandem undulator. The tandem undulator radiation consists of pairs of light wave packets [6], and the longitudinal coherence within each light wave packet pair is used to realize time-domain interferometry.

The time delay between each light wave packet pair is the key parameter of time-domain interferometry and can be adjusted using phase shifter magnets that form a chicane of the electron trajectory between the two undulators. In time-domain interferometry experiments, the temporal precision of the time delay should be better than or at least comparable to the optical periods of light. Thus, its required accuracy in the temporal precision is as short as attoseconds in the XUV regime. While an autocorrelation measurement is a simple way to optically observe the time delay with attosecond precision [6], it is difficult to construct an autocorrelation interferometer in the XUV regime.

In this study [7], we show that frequency-domain spectroscopy enables us to determine the time delay between a light wave packet pair with an accuracy on the order of attoseconds. Figure 1 presents the frequency-domain tandem undulator spectra observed at three different current conditions of the phase shifter magnets. Both undulators were set to generate radiation with central photon energies of approximately 24 eV. These spectra exhibit fringe structures whose envelopes delineate the radiation spectra of the individual undulators. One finds that the number of fringes increases as increasing the phase shifter current (i.e., as increasing the time delay between the light wave packets).

The fringe structures result from the optical interference between two light wave packets, exhibiting a spacing of h/τ [7]. Here, h is Planck's constant, and τ is the delay time between a light wave packet pair. To accurately determine the time delays from the fringe structures, we use a fitting function considering the radiation spectra of the individual undulators [7]. The value determined by fitting to each frequency-domain spectrum is given in the corresponding panel of Fig. 1. The error in the frequency-domain determination can be estimated to be about 1.5% [7]. This study proves that the time delay between XUV light wave packet pairs can be determined by frequency-domain spectroscopy with an accuracy on the order of attoseconds.

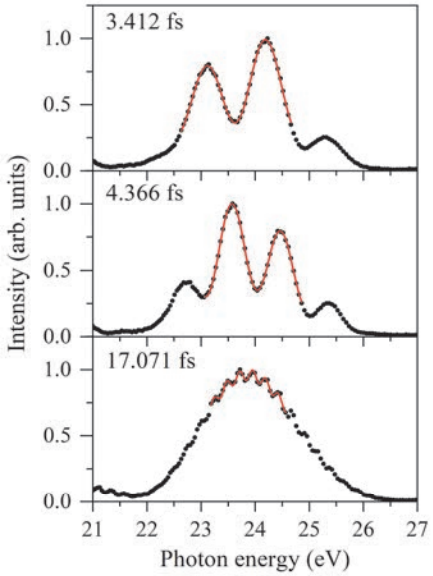

Fig. 1. Frequency-domain tandem undulator spectra (dots) measured at three different phase shifter conditions, and fitting results (red solid line).

[1] Y. Hikosaka *et al.*, Nat. Commun. **10** (2019) 4988; **12** (2021) 3782.
[2] T. Kaneyasu *et al.*, Phys. Rev. Lett. **123** (2019) 233401.
[3] T. Kaneyasu *et al.*, New J. Phys. **22** (2020) 083062.
[4] T. Kaneyasu *et al.*, Phys. Rev. Lett. **126** (2021) 113202.
[5] T. Kaneyasu *et al.*, Sci. Rep. **13** (2023) 6142.
[6] T. Kaneyasu *et al.*, Sci. Rep. **12** (2022) 9682.
[7] Y. Hikosaka *et al.*, Sci. Rep. **13** (2023) 10292.

BL1U

Diffraction of Optical Vortex from Undulator

Y. Nishihara[1], M. Shimada[2,3], H. Miyauchi[3,2], K. Matsuo[1,3] and M. Katoh[3,1,4]
[1]*School of Science, Hiroshima University, Higashi-Hiroshima 739-8526, Japan*
[2]*High Energy Accelerator Research Organization (KEK), Tsukuba 305-0801, Japan*
[3]*Hiroshima Synchrotron Radiation Center, Hiroshima University, Higashi-Hiroshima 739-0046*
[4]*UVSOR Synchrotron Facility, Institute for Molecular Science, Okazaki 444-8585, Japan*

Optical vortex is a light beam possessing helical wavefront and carrying orbital angular momentum [1]. It has been attracting researchers in various field and its applications has been being explored [2]. To make experimental studies, various methods have been developed to convert normal light beam to optical vortex beam by using specially designed optical devises or elements [2]. On the other hand, it was theoretically shown that radiation from an electron in circular motion with a relativistic speed has vortex property [3]. Electron motion in a helical undulator radiation may be regarded as combination of mildly relativistic circular motion and ultra-relativistic drift motion along the rotation axis, which is identical with the undulator axis in this case. Therefore, helical undulator radiation has vortex property such that the fundamental component is circularly polarized plane wave and the higher harmonics are circularly polarized but optical vortex with helical wavefront [4].

Undulator vortex radiation can cover much wider wavelength range than vortex light beam based on conventional light sources. In particular, it can cover the vacuum ultraviolet and X-ray wavelength ranges, where the light and matters show strong interactions. Undulator vortex radiation may play important roles in the material science or the life science.

When we apply the undulator vortex radiation to some experiments, it is desirable to have a method for observing the helicity and the topological charge of the vortex beam at various position along the beam-line. It is well known that optical vortex shows interesting diffraction patterns for various apertures [5, 6, 7]. We may obtain information on the vortex property from the diffraction patterns. Among these, diffraction from triangular aperture seemed most feasible for this purpose, because it gives the information on the vortex property as a visible form which is easily identified by eye [3].

To make a systematic study on the triangular diffraction, we have prepared triangular aperture of several size. The experiment was carried out at BL1U of UVSOR-III storage ring. This beam-line equipped with APPLE-II type undulator. By setting it in the helical mode with the fundamental wavelength at 710 nm, the second harmonic radiation at 355 nm was extracted to the air. By using conventional CCD camera with a bandpass filter centered at 355 nm with a moderate bandwidth, we made observation on the diffraction pattern.

Some of the results are shown in Figure 1. We succeeded in observing the characteristic pattern which shows the helicity and the topological charge of the vortex undulator radiation. We also observed the diffraction pattern for the fundamental undulator radiation tuned at 355 nm, which is not vortex but normal plane wave. The result was also shown in Figure 1, which is as expected for normal plane wave.

From the experiment, we found that the size of the triangular aperture should be fitted to the size of the vortex beam. We also found the tolerance of the alignment of the center of the vortex and the aperture. The details of these results were presented elsewhere [8].

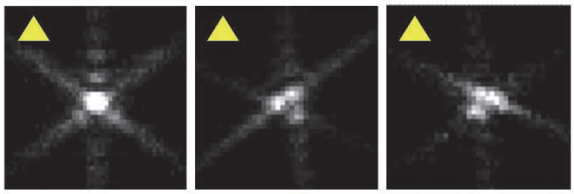

Fig. 1. Diffraction by triangular aperture of helical undulator radiation observed at UVSOR BL1U, for 1st harmonic (left) and 2nd harmonic radiation (center and right, the helicity is reversed). The wavelength is centered at 355 nm.

[1] L. Allen *et al*., Phys. Rev. A: At. Mol. Opt. Phys. **45** (1992) 8185.
[2] Y. Shen *et al*., Light Sci. Appl. **8** (2019) 90.
[3] M. Katoh *et al*., Phys. Rev. Lett. **118** (2017) 094801.
[4] M. Katoh *et al*., Sci. Rep. **7** (2017) 6130.
[5] J.M. Hickmann *et al*., Phys. Rev. Lett. **105** (2010) 053904.
[6] G. G. C. Berkhout *et al*., Phys. Rev. Lett. **101** (2008) 100801.
[7] H. I. Sztul *et al*., Opt. Lett. **31** (2006) 999.
[8] Y. Nishihara, Bachelor thesis (Hiroshima University), (2024).

BL2A

Evaluation of CMOS Detector Abord the Sounding Rocket Experiment FOXSI-4 for a Solar Flare Observation in X-rays

N. Narukage [1,2], R. Shimizu[2,3], Y. Sato[2,1] and S. Kashima[3]

[1]*National Astronomical Observatory of Japan (NAOJ), Mitaka, 181-8588, Tokyo, Japan*

[2]*The Graduate University for Advanced Studies, SOKENDAI, Hayama, 240-0193, Kanagawa, Japan*

[3]*Institute of Space and Astronautical Science (ISAS), Japan Aerospace Exploration Agency (JAXA), Sagamihara, 252-5210, Kanagawa, Japan*

The solar corona is full of dynamic phenomena such as solar flares. The understandings of these phenomena have been progressing step-by-step with the evolution of the observation technology in EUV and X-rays from the space. But there are fundamental questions remain unanswered or haven't even addressed so far. Our scientific objective is to understand underlying physics of the dynamic phenomena in the solar corona, covering some of the long-standing questions in solar physics such as particle acceleration in flares and coronal heating. To achieve this objective, we identify the imaging spectroscopy (the observations with spatial, temporal and energy resolutions) in the soft X-ray range (from ~0.5 keV to ~10 keV) is a powerful approach for the detection and analysis of energetic events [1]. This energy range contains many lines emitted from below 1 MK to beyond 10 MK plasmas plus continuum component that reflects the electron temperature.

The soft X-ray imaging spectroscopy is realized with the following method. We take images with a short enough exposure to detect only single X-ray photon in an isolated pixel area with a fine pixel Silicon detector. So, we can measure the energy of the X-ray photons one by one with spatial and temporal resolutions. When we use a high-speed soft X-ray camera that can perform the continuous exposure with a rate of more than several hundred times per second, we can count the photon energy with a rate of several 10 photons / pixel / second. This high-speed exposure is enough to track the time evolution of spectra generated by dynamic phenomena in the solar corona, whose lifetimes are about form several ten seconds to several minutes. For the first imaging spectroscopic observation of the solar corona in soft X-ray range, we launched a NASA's sounding rocket (FOXSI-3) on September 7th, 2018 and successfully obtained the unprecedented data [2] using a high-speed X-ray camera [3] with a back-illuminated CMOS detector [4].

Based on the success of FOXSI-3, we will launch the sounding rocket experiment FOXSI-4 in April 2024, which will conduct the world's first X-ray focusing imaging spectroscopic observation of a solar flare. This FOXSI-4 uses a fully depleted CMOS detector with a silicon thickness of 25 microns, which provides high sensitivity to high-energy X-rays.

In FY2023, we evaluated this CMOS detector by emitting the monochromatic X-rays with a resolution of 25 eV from 0.8 keV to 4.5 keV at UVSOR BL2A and 4.5 keV to 10 keV at SPring-8 BL20B2.

Figure 1 is the evaluated response matrix, which represents what kind of signal the detector outputs when monochromatic X-rays are incident on it. The color shows the fractional distribution of the output signal values (horizontal axis) when X-rays with the energy indicated on the vertical axis are incident. The features shown by (1), (2) and (3) are the main peak, silicon escape and silicon emission, respectively. The main peak is proportional to the energy of the incident X-rays, and its full width at half maximum is small and its intensity is higher than the other peaks. These facts mean that this detector has excellent performance in X-ray energy measurement.

Although a response matrix is indispensable for analyzing observation data, this is the first time that such a detailed matrix has been obtained by actual measurements. This matrix is extremely useful for the analysis of solar flare data obtained by FOXSI-4.

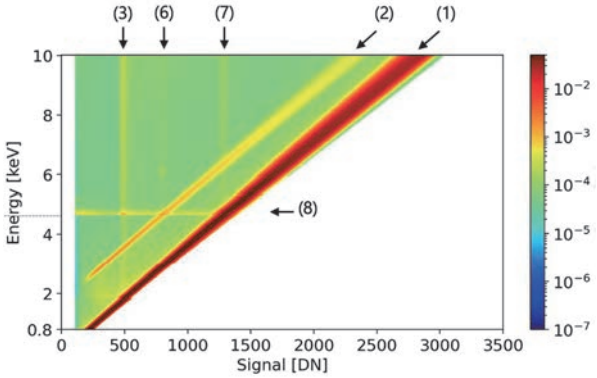

Fig. 1. Evaluated response matrix of the CMOS detector abord the sounding rocket experiment FOXSI-4.

[1] N. Narukage *et al.*, arXiv:1706.04536 (2017).
[2] N. Narukage and S. Ishikawa, UVSOR Activity Report **46** (2019) 36.
[3] S. Ishikawa *et al.*, Nucl. Instrum. Methods Phys. Res., Sect. A **912** (2018) 191-194.
[4] N. Narukage *et al.*, Nucl. Instrum. Methods Phys. Res., Sect. A **950** (2020) 162974.
[5] N. Narukage, UVSOR Activity Report **49** (2022) 42.

BL2A

Development of Operando Measurement of Battery Materials by Soft X-ray Absorption Spectroscopy using Sample Transfer Vessel

E. Kobayashi[1] and A. Inoishi[2]
[1]*Kyushu Synchrotron Light Research Center, 8-7 Yayoigaoka, Tosu, Saga 841-0005, Japan*
[2]*Institute for Materials Chemistry and Engineering, Kyushu University*
6-1 Kasuga-koen, Kasuga-Shi, Fukuoka 816-8580, Japan

In recent years, secondary batteries have been used in a wide range of fields such as mobile phones, and electric vehicles, and further improvements in performance are desired. Most battery materials are sensitive against atmospheric components such as oxygen, carbon monoxide, and moisture, so they must be handled without exposure to the atmosphere. So far, we have developed a sample transfer vessel that can transport the sample to the analyzer without exposing it to the atmosphere [1, 2]. In addition, when performing analysis using soft X-ray absorption spectroscopy, light elements contained in battery materials have a wide range of absorption edge energy, from lithium to chlorine, so there are cases where measurement cannot be performed using a single beamline or cannot be handled within the facility. Therefore, we have developed a device based on the sample transfer vessel [1, 2] that can measure soft X-ray absorption spectra across beam lines or facilities without exposure to the atmosphere. Furthermore, in order to more accurately evaluate the reactions occurring in batteries, it is important to measure the conditions in which the reactions are actually occurring. Therefore, we are developing a device that can measure soft X-ray absorption spectra across a beamline or facility without exposure to the atmosphere, with the addition of a function that can apply voltage to the sample.

Figure 1 is a photograph of the developed transfer vessel installed on the beamline. The device was attached to the conflat flange (CF) 70 port at the end of the beam line. The silicon drift detector (SDD), which detects soft X-rays emitted from the sample, was installed at 90 degrees to the direction of light incidence. Figure 2 is a photograph of the sample holder. The front and back surfaces of the sample are insulated, and a potential can be applied to each of these surfaces. Using this vessel, we observed the soft X-ray absorption spectra of all-solid-state batteries during charging and discharging. As a result, it was confirmed that the chemical state of the battery changes due to charging and discharging.

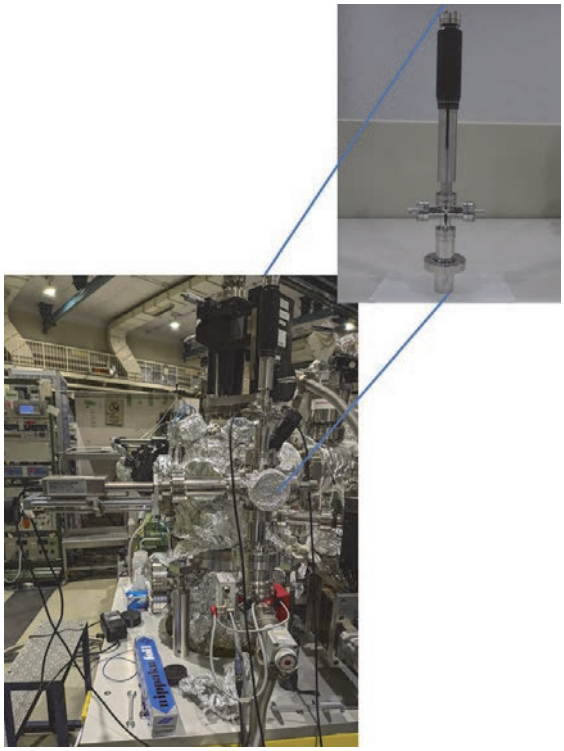

Fig. 1. Photograph of the developed transfer vessel.

Fig. 2. Photograph of the sample holder.

[1] E. Kobayashi *et al*., Japanese Patent No. 5234994.
[2] E. Kobayashi *et al*., J. Surf. Anal. **19** (2012) 2.

BL5B

Reflectivity Measurement on SiC/Mo/Si Multilayer Coated Mirrors for Future Planetary Exploration

M. Kuwabara[1], Y. Suzuki[2], A. Yamazaki[3] and I. Yoshikawa[4]

[1]*Department of Physics, College of Science, Rikkyo University, Tokyo 171-8501, Japan*

[2]*Institute of Space and Astronautical Science, Japan Aerospace Exploration Agency, Kanagawa 252-5210, Japan*

[3]*Department of Earth and Planetary Science, Graduate School of Science, The University of Tokyo, Tokyo 113-0033, Japan*

[4]*Department of Complexity Science and Engineering, Graduate School of Frontier Science, The University of Tokyo, Chiba 277-8561, Japan*

Optical observations of planetary atmospheres have been conducted across various wavelength ranges. Particularly, ultraviolet (UV) light is notably useful in planetary science for acquiring spatial structure and temporal evolution of planetary upper atmospheres. However, detection of UV light through ground-based observations is hindered by absorption caused by the Earth's atmosphere.

Periodic multilayer coating technique has been developed for normal incidence optics in the soft X-ray and extreme ultraviolet (EUV) spectral regions. By applying multiple materials with different complex refractive indices in layers on the surface of a mirror, the reflectivity can be dramatically improved through the interference of reflected light at each interface.

In the field of planetary science, this technique for EUV radiation has been utilized in many missions. High reflectivity multilayer coatings for He II radiation (30.4 nm) have been developed for several applications, among which Mo/Si multilayer coated mirrors have been widely used for He II observations due to their high stability [1]. However, their reflectivity reaches at best approximately 18%. In recent years, with the increasing opportunities for missions by ultra-small spacecraft, there has been a demand for the development of multilayer coatings with higher reflectivity. To achieve higher reflectivity, Mg/SiC multilayer coated mirrors have also been developed. While Mg/SiC mirrors achieve reflectivity exceeding 30% at 30.4 nm [2], instability due to the deliquescence of Mg hampers their practical application.

In this study, we developed multilayer mirrors with a new SiC/Mo/Si coating expected to achieve higher reflectivity than conventional ones. We evaluated their reflectivity for s-polarized and p-polarized light, respectively.

Figure 1 shows the experimental configuration for reflectivity measurement for p-polarized light. Measurements have been performed on two mirrors (#1 and #2) with identical design parameters but different production lots. Five stacked microchannel plates (MCPs) and a resistive anode encoder (RAE) are assembled and used as a photon detector. A goniometer is moved to measure reflectivity for an incident angle of 20 degrees. For reflectivity measurements for s-polarized light, the phase of the goniometer relative to the diffracted light is changed by 90 degrees.

The initial results of the reflectivity measurements of the SiC/Mo/Si multilayer coated mirrors are shown in Figure 2. The newly developed SiC/Mo/Si mirrors have been found to have reflectivity potentially comparable to or exceeding that of the conventional Mo/Si mirrors. However, there are some uncertainties in these preliminary findings, highlighting the need for further detailed analysis in future studies.

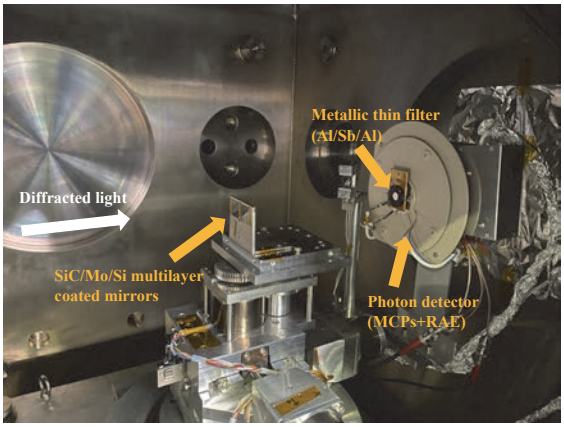

Fig. 1. Configuration of the experiment for reflectivity measurement for p-polarized light.

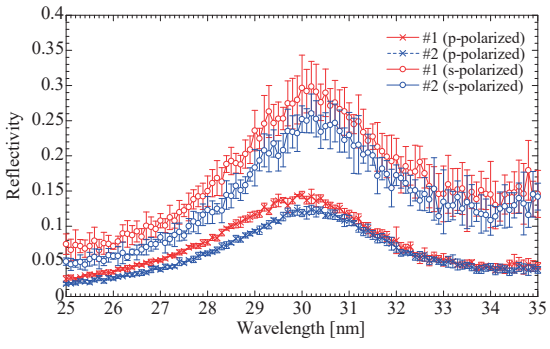

Fig. 2. Reflectivity of the SiC/Mo/Si multilayer coated mirrors.

[1] I. Yoshikawa *et al.*, Earth Planets Space **60** (2008) 407.

[2] M. Kuwabara, Doctoral thesis (The University of Tokyo, 2018).

BL5B

Radiometric Calibration of a High-Resolution EUV Spectrometer

T. Kawate[1,2], H. A. Sakaue[1] and C. Suzuki[1,2]
[1]*National Institute for Fusion Science, Toki 509-5292, Japan*
[2]*The Graduate University for Advanced Studies (SOKENDAI), Toki 509-5292, Japan*

Understanding the structures of Unresolved Transition Array (UTA) observed in emission spectra from many-electron atoms is essential for many application fields, for example, developing the future light sources of semiconductor lithography and impurity transport in magnetically confined fusion plasmas. To model and validate the fine structures of the UTA spectra especially from tin at around 13.5 nm, gadolinium and terbium at around 6.8 nm, and tungsten at around 5.0 nm, we develop a high-resolution and high-throughput extreme ultraviolet spectrometer. Since UTA spectra span wide wavelength ranges, the radiometric calibration as a function of wavelength is crucial for the newly developed spectrometer.

In the UVSOR experiments, we measured the quantum efficiency of the CCD camera and the diffraction efficiency of the gratings for the high-resolution spectrometer using the calibration beamline [1] installed on BL5B. The CCD camera, PIXOS-XO:400B (Teledyne Princeton Instruments), was mounted on the backside of the chamber (Fig. 1(a)) with an XY-axis translation stage. We scanned the wavelengths using the monochromator in the beamline as well as the positions of the beam onto the detector using the translation stage. By inserting the calibrated photodiode AXUV100 in the middle of the beamline, we obtained the quantum efficiency of the CCD as a function of wavelength and position on the detector. The obtained quantum efficiency shows good agreement with the one provided by the manufacturer.

The gratings were a custom-made laminar type with spherical varied-line spacing manufactured by Shimadzu Corporation. The central groove density and the ruled area were 2300-line/mm and 90 x 30-mm^2, respectively. We designed the gratings to measure ~13 nm for first-order diffraction and 4-8 nm for second-order diffraction. It was mounted on the sample holder in the calibration chamber (Fig. 1(b)). To compare the diffraction efficiency under different polarization conditions, we performed experiments by changing the axis of coaxial rotation of the goniometer to vertical and horizontal directions. The measured diffraction efficiency is shown in Fig. 2. Although the difference between the polarization directions of the beam is not significant, the averaged efficiencies over the vertical and horizontal configurations agree with the calculation by PCGrate-SX software version 6.6 (I.I.G. Inc.).

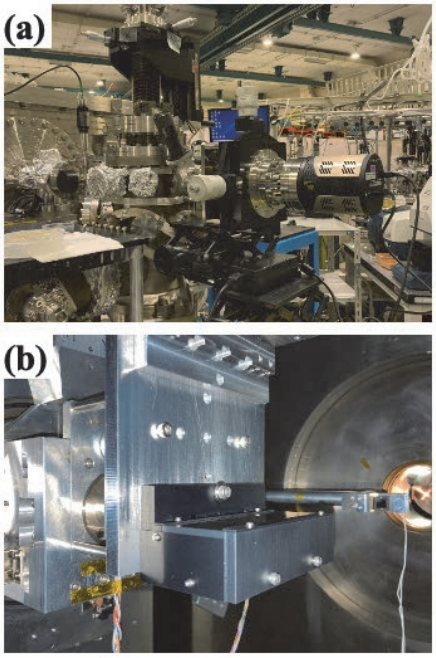

Fig. 1. Photos of the (a) CCD and (b) grating mounted on/in the calibration chamber.

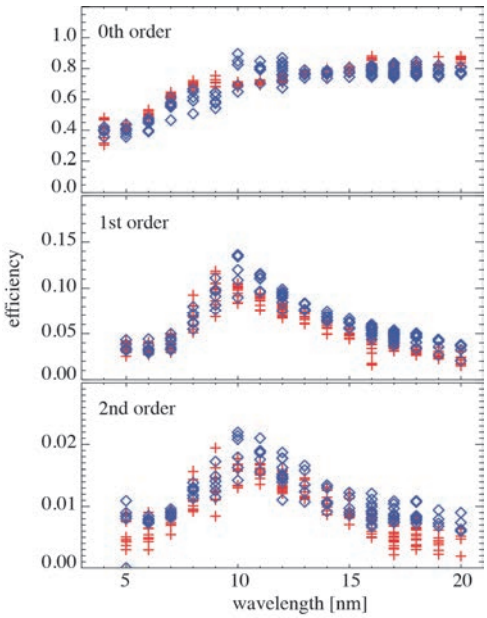

Fig. 2. Measured diffraction efficiencies of the grating with the axis of coaxial rotation of horizontal (blue diamond) and vertical (red cross) directions. The vertical scattering of the data points represents the efficiency at different positions on the grating.

[1] M. Sakurai *et al.*, Rev. Sci. Instrum. **60** (1989) 2089.

BL5B

Calibration of Position-Sensitive Microchannel Plate Detectors

S. Matoba[1], S. Kanda[1], H. Ohshita[1], K. Hirata[2], H. Iwayama[3, 4] and T. Kaneyasu[5]

[1]*Institute of Materials Structure Science, KEK, Tsukuba 305-0801, Japan*

[2]*National Institute of Advanced Industrial Science and Technology, Tsukuba, 305-8569, Japan*

[3]*UVSOR Synchrotron Facility, Institute for Molecular Science, Okazaki 444-8585, Japan*

[4]*School of Physical Sciences, The Graduate University for Advanced Studies (SOKENDAI), Okazaki 444-8585, Japan*

[5]*SAGA Light Source, Tosu 841-0005, Japan*

We are developing a compact imaging system that can be inserted into the beamline to monitor neutron and muon beams. In this system, a carbon resistive anode is placed at the rear of the microchannel plate (MCP), and the position of the incident particle can be detected. The resistive anode encoder has a square shape, and charge is extracted from the four corners. The coordinates of the center of charge on the resistor anodes are derived from

$$x/L = (Q_2+Q_3)/(Q_1+Q_2+Q_3+Q_4),$$
$$y/L = (Q_3+Q_4)/(Q_1+Q_2+Q_3+Q_4), \quad (1)$$

where $Q_i (i = 1, 2, 3, 4)$ represents the amount of charge collected by each electrode on the resistive anode and L represents the distance between adjacent vertices, as shown in Fig. 1. Charges extracted from the four corners are measured by a 4-channel digitizer with 500MHz. The measurement was performed under the condition that the yield was limited to a few hundred counts per second and that no simultaneous injection into the MCP occurred. The signal from ch1 was used as the trigger, and the position was calculated according to Equation 1 by capturing the electric charge from each channel within 20 nanoseconds before and after the trigger.

We calibrated the position of the particle detection position of the system using 122 nm light at BL5b. The synchrotron radiation was incident on the microchannel plate through the attenuation filter and a 3 mm circular slit. Figure 2 shows the distribution of light detection positions in the horizontal (x) and vertical (y) directions. Figure 3 shows the position distribution of the noise signal when the shutter is closed. The reconstructed noise positions are not uniform but have a certain distribution. However, since the position distribution is not peaky, the effect on the analysis of the illuminated data is small. By using the RAE charge output as a self-trigger, the beam spot could be determined with high S/N.

From the above, it was confirmed that the constructed detector system is working properly. In the future, we plan to measure the optical detection efficiency using this system.

I would like to thank Mr. E. Nakamura for his great support of this experiment.

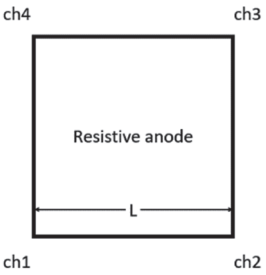

Fig. 1. Schematic of resistive anode.

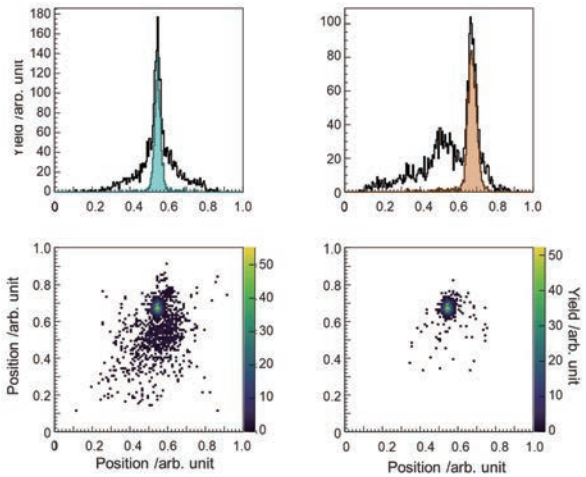

Fig. 2. Signal position distribution. X and Y distributions are shown above, respectively. Colored signals are those synchronized with the light trigger. The lower panel is a two-dimensional map. The right panel shows the signal synchronized with the light trigger.

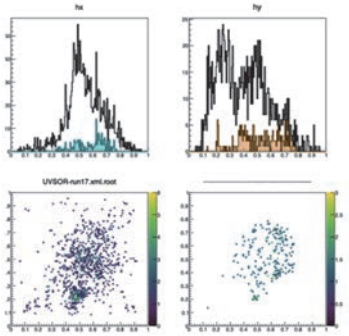

Fig. 3. Signal position distribution with shutters closed.

BL6U

Development of a Program to Analysis Multi-Dimensional Data of the Photoelectron Momentum Microscopy

S. Tanaka
SANKEN, Osaka University, Ibaraki 464-0056, Japan

The photoelectron momentum microscopy (PMM) is a revolutionary experimental method in which both the angle-resolved photoelectron spectroscopy (ARPES) and the photoemission electron microscopy (PEEM) techniques are combined in highly sophisticated way[1]. The PMM operated with the synchrotron radiation beamline provides huge amount of data in multi-dimensions, i.e., momentum, binding energy, position in the real space, polarization, photon energy, etc[2]. However, the distributed program from the manufacture has limited functions and not very convenient to use. Therefore, the development of a new program which enable us to conveniently analyze the multi-dimensional data of the PMM is highly desired.

The program now under developing holds following benefits:

1) The program is written in the Python language, which is a standard language in many fields including the data science, and runs under multiple OSs (Windows 10/11, Mac OS, and Linux).

2) The whole program consists of self-standing functional programs, *i.e.*, a data-reading, a 2D-data analysis, a 3D-data analysis (Fig.1), a 3D-volumetric presentation, a multiple-peak-fitting, a Fermi-Dirac fitting, a curvature method including the second-derivative to clarify the structure in the 2D intensity map, *etc.* Adding to these procedures commonly used in the angle-resolved photoelectron spectroscopy, analytic tools specified for the PMM with the synchrotron radiation are provided (Fig.2).

3) The program can be used as a data-format converter. Raw data can be obtained directly from an "sle" file which is produced by the experimental program. Then, these are calculated for the analysis (integration, calibration, conversion, smooth, *etc.*), These can be saved not only in "npy" (the binary format of python) file but also in "csv" ("comma-separated value" in ascii format), "h5" (the HDF format), "ibw" (igor binary wave), "itx" (igor text) formats. Then, users can complete the figures by using their own programs.

An example of working windows of the program (running on the Mac OS) are shown in Figs. 1 and 2. The next function will be a reading and analyzing the result of the spin-resolved measurements.

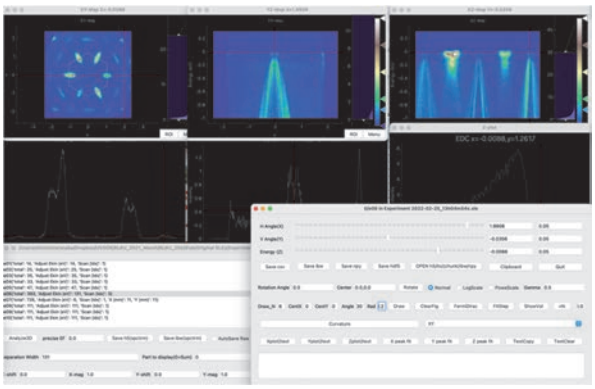

Fig. 1. Windows of the 3D-analysis mode. 2D intensity maps along k_x,k_y, k_x-BE (Biding Energy) and k_y-BE are shown together with intensity plots as functions of k_x, k_y and BE. The points of plotting can be easily chosen using slide bars.
The sample is $TiSe_2$ at 30K.

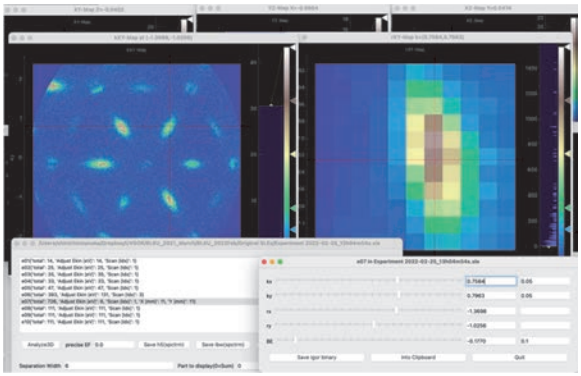

Fig. 2. Windows of the ARPES/microscopy analyzing program. Left window shows the photoelectron intensity map in the momentum space, and the right one shows that in in the real space. The data acquisition point is shown by the crossing point of the red line in both spaces. In this case, the sample is TiSe2 as well as in Fig.1, and the real space distribution is mainly affected by the angular distribution of the photoelectron because the sample surface is not perfectly flat.

[1] F. Matsui *et al.*, Rev. Sci. Instrum. **94** (2023) 083701.
[2] K. Hagiwara *et al.*, J. Synchrotron Radiat. **31** (2024) 540.

BL6U

Numerical Correction of α² Aberration on PMM Imaging at BL6U

R. Sagehashi[1], K. Hagiwara[2], S. Kera[1,2] and F. Matsui[2]
[1]*Department of Photo-Molecular Science, Institute for Molecular Science, Okazaki 444-8585, Japan*
[2]*UVSOR Synchrotron Facility, Institute for Molecular Science, Okazaki 444-8585, Japan*

Hemispherical deflection analyzers (HDAs) are often used for angle-resolved photoelectron spectroscopy measurements to achieve high energy resolution by acquiring photoelectrons as a two-dimensional (2D) function of kinetic energy versus angle. Furthermore, HDA allows energy-selected imaging the 2D angular distribution of electrons entering the HDA entrance aperture. However, the pass energy of electrons varies with the entrance angle along the energy dispersion axis (α). The effective pass energy is expressed by the following formula:

$$E_{pass}(\alpha)/E_{pass}(0°) = (1-\sin^2\alpha)^{-1} \approx (1+\alpha^2). \quad (1)$$

This phenomenon is called α² aberration [1]. Due to this aberration, imaging results such as band structure and photoelectron angular distribution are accompanied by energy shift. When HDA is used for imaging angle-resolved spectra, the α² aberration reduces the energy resolution. On the other hand, when using HDA to image a 2D angular distribution, α² aberration occurs at different detector positions. The photoelectron momentum microscope (PMM) installed at BL6U uses this type of detection [2]. In this case, since the influence of α² aberration can be removed as described later, the energy resolution is not affected.

Figure 1 shows the experimental data of the band structure of Au(111) surface obtained by PMM at BL6U in 2024.02. It showed clear energy shift of Fermi level along k_α axis (the energy axis in HDA) due to α² aberration. This energy shift can be fitted by second polynomial function. In order to detect Fermi level (E_F) at every spectrum, they were fitted by Fermi-Dirac function:

$$f(E) = (1+\exp((E-E_F)/k_BT))^{-1}. \quad (2)$$

By using these results, E_F at each angle α can be evaluated. As a result, the energy difference between maximum and minimum was around 25 meV. Next, $E_F(k_\alpha)$ was fitted by second polynomial function. In this case, the following function was obtained as fitting function:

$$E_F(k_\alpha) = -7.34k_\alpha^2-5.78k_\alpha+1.60. \quad (3)$$

Finally, every spectrum was readjusted considering with this equation. Figure 2 indicates original data of photoelectron momentum pattern at Fermi level (a) and corrected pattern (b). Comparing them, the pattern after correction was clearly seen at $k_\alpha < -1.8$ Å^{-1} and $+1.8$ Å$^{-1} < k_\alpha$ more than the original data.

We also performed same analysis on the data about Au(111) taken in 2022.01. As a result, the coefficient of k_α^2 in the fitting function became -1.69, which is less than a quarter of the data in 2024.02. The pass energy were 20 eV and 50 eV in 2022 and 2024, respectively. According to Eq. (1), the α² aberration get bigger when pass energy becomes bigger. In 2022, the single HDA was used at BL6U, while double HDA system is installed now. Since it is equivalent to doubling the radius of HDA, the α² aberration also becomes bigger. On the other hand, there was little difference of energy resolution after aberration correction between 2022 and 2024, both values were around 15 meV. Nevertheless, the transmission of HDA is related to the squared pass energy. As a result, the double HDA allows PMM measurements approximately 4 times more efficiently than the single HDA in this case.

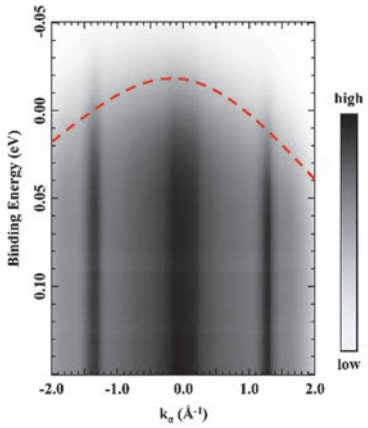

Fig. 1. The band structure of Au(111) surface around valence band obtained by PMM measurement at BL6U. (Red dashed line indicates α² aberration.)

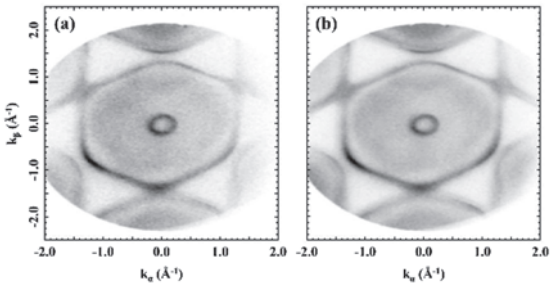

Fig. 2. Photoelectron momentum pattern of Au(111) surface (Fig. 1) at Fermi level. (a) Before correction. (b) After correction.

[1] C. Tusche, A. Krasyuk and J. Kirschner, Ultramicroscopy **159** (2015) 520.
[2] F. Matsui *et al.*, Jpn. J. Appl. Phys. **59** (2020) 067001.

BL6U, BL7U

Development of Dual-Beamline Photoelectron Momentum Microscope

K. Hagiwara[1], E. Nakamura[1], S. Makita[1], S. Suga[2], S. Tanaka[2], S. Kera[1, 3] and F. Matsui[1, 3]
[1]*UVSOR Synchrotron Facility, Institute for Molecular Science, Okazaki 444-8585, Japan*
[2]*SANKEN, Osaka University, Mihogaoka 8-1, Ibaraki 567-0047, Japan*
[3]*School of Physical Sciences, The Graduate University for Advanced Studies (SOKENDAI), Okazaki 444-8585, Japan*

We have developed a unique dual-beamline photoelectron spectroscopy experimental station combined with a state-of-the-art photoelectron momentum microscopy (PMM) analyzer [1]. PMM combines a photoemission electron microscope (PEEM)-type objective lens and an energy-filtering hemispherical deflection analyzer. PMM allows photoelectron imaging in real and momentum spaces, facilitating electronic structure analyses in local μm-scale domains. PMM has been installed at the soft X-ray beamline BL6U of UVSOR synchrotron facility [2, 3]. In 2023, by branching the vacuum ultraviolet (VUV) beamline BL7U [4], a VUV beam was successfully guided to the same sample position as the soft X-ray beam from BL6U [1] as shown in Fig. 1. This upgrade allowed us to use wide-energy photons $h\nu$ = 6 -30 and 40 - 800 eV in the PMM experimental station. The VUV beam with variable polarization in the normal-incidence geometry now became available. The detailed experimental geometry of PMM is illustrated in Fig. 2. We note here that momentum-resolved photoelectron spectroscopy in such normal-incidence geometry is currently only available with this UVSOR PMM. Such highly symmetric photoemission geometry with normal incidence offers direct access to atomic orbital information via photon polarization-dependent transition-matrix-element analysis.

We measured the photoelectron momentum distribution of the Au(111) surface using horizontally and vertically polarized light from BL7U in addition to p-polarized light from BL6U as shown in the two insets of Fig. 2. Colored intensities show contribution of corresponding photon polarizations.

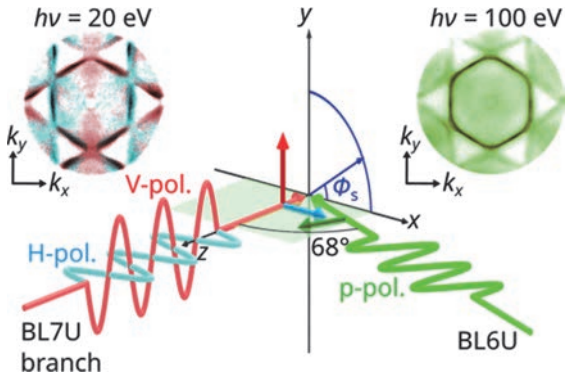

Fig. 2. Experimental geometry of the PMM station with two beams. p-polarized light from BL6U is incident in the *x*-*z* plane at an angle of 68º from the sample surface normal (*z*) axis. Here, the plane of incidence (*x*-*z* plane) is represented by the green horizontal plane. Horizontally and vertically polarized light from the BL7U branch passes along the surface normal (*z*) axis. Samples can be rotated in-plane at an angle of ϕ_s. The two insets show the measured photoelectron momentum patterns of the Au(111) surface with various photon polarizations.

[1] K. Hagiwara *et al*., J. Synchrotron Radiat. **31** (2024) 540.
[2] F. Matsui *et al*., Jpn. J. Appl. Phys. **59** (2020) 067001.
[3] F. Matsui *et al*., Rev. Sci. Instrum. **94** (2023) 083701.
[4] S. Kimura *et al.,* Rev. Sci. Instrum. **81** (2010) 053104.

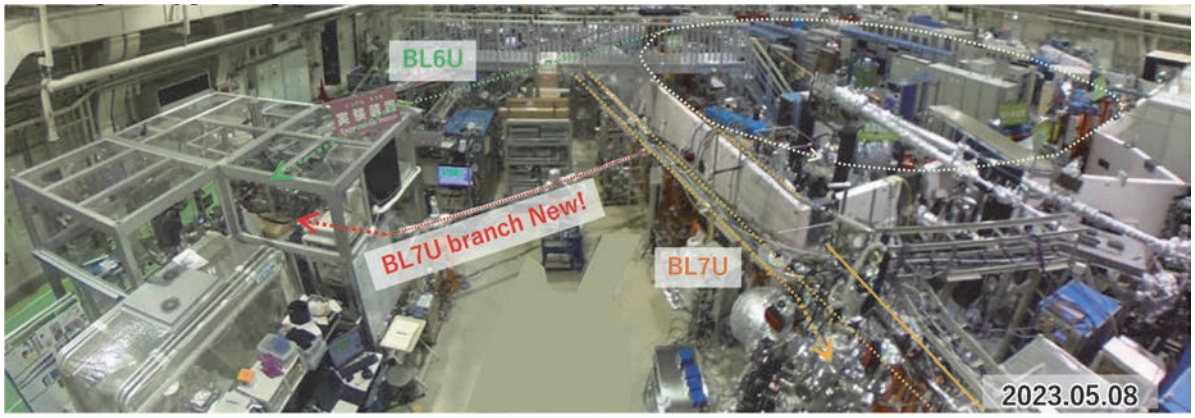

Fig. 1. Photograph of beamline BL6U, BL7U, and the newly constructed BL7U branch.

BL6B

Development of a Uniaxial Pressure Cell for Infrared and ARPES Measurements

H. Watanabe[1,2], H. Ishida[2] and S. Kimura[1,2,3]

[1]*Graduate School of Frontier Biosciences, Osaka University, Suita 565-0871, Japan*

[2]*Department of Physics, Graduate School of Science, Osaka University, Toyonaka 560-0043, Japan*

[3]*Institute for Molecular Science, Okazaki 444-8585, Japan*

III-1

Pressure is one of the most fundamental external perturbations that control interactions within materials. Numerous physical properties have been measured under applied pressure using diamond anvil cells and piston-cylinder cells. In these experiments, photoelectron spectroscopy (PES) and wide-range optical measurements are prevented due to the requirement of window materials such as diamond and sapphire to apply hydrostatic pressure. Such optical measurements are required to observe the change in the electronic structure with pressure. Then, we developed a compact pressure cell without window materials, a uniaxial pressure cell (UPC) with a piezoelectric actuator (PA) control for PES and optical measurements. The UPC was designed for general spectroscopic measurements, including infrared spectroscopy and ARPES measurements.

So far, angle-resolved PES (ARPES) using a uniaxial stage using the difference in expansion coefficient of metals with temperature has already been reported [1]. Still, it is difficult to control temperature and pressure independently. On the other hand, a PA-based UPC has already been developed and supplied by Razorbill Instruments [2]. Owing to the large size, however, it is difficult to mount on the Oxford-type sample holder (sample area: 10×10 mm^2) for optical measurements and the Omicron-type holder (13×13 mm^2) for ARPES.

As a practical demonstration of our innovation, we have successfully developed a prototype UPC that can be mounted on a widely used cryostat of MicrostatHe (Oxford Instruments) and the Omicron holder for ARPES. The UPC can easily apply uniaxial pressure using a PA by applying voltage. Figure 1(a) showcases the UPC (10×15 mm^2) mounted on the MicrostatHe sample stage (19×19 mm^2). The UPC consists of three PAs; one of the three (the other two) is used for pressurizing (pulling). The metallic parts, fabricated by the Equipment Development Center of the Institute for Molecular Science, are connected to PAs with Stycast (LOCTITE, Henkel Co.). The position of the center stage can be changed with the varying PA voltage, as shown in Fig. 1(b). The stage shift per PA voltage is 30 nm/V, consistent with the PA standard. This successful demonstration confirms the practicality and effectiveness of our UPC.

Building on the success of our prototype, we envision creating a new UPC using PA that can be utilized at low temperatures. Our plans also include measuring pressure at low temperatures, a crucial step in expanding the practical applications of the UPC.

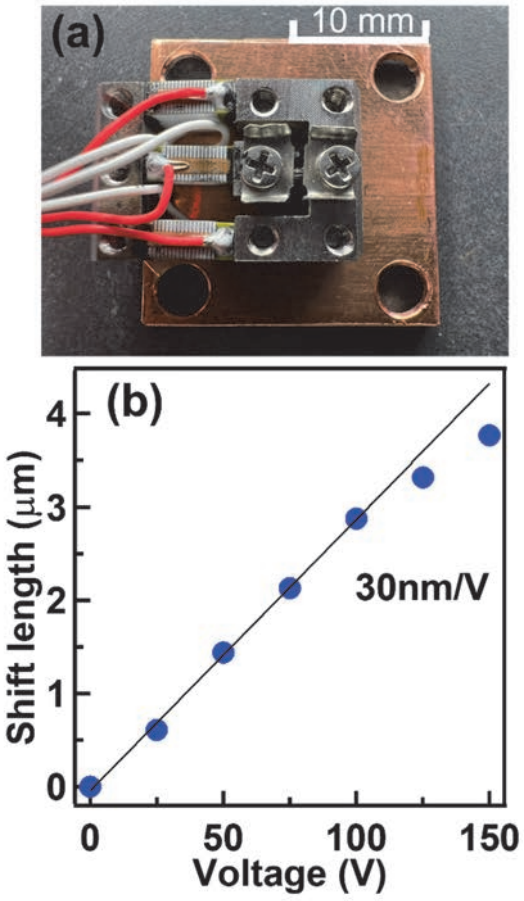

Fig. 1. Photograph of the UPC mounted on the MicrostatHe sample stage (a) PA voltage dependence of the shifted length of stage (b)

[1] V. Sunko *et al*., npj Quantum Mater. **4** (2019) 46.
[2] M. E. Barber *et al*., Rev. Sci. Instrum. **90** (2019) 023904.

Others

Performance Evaluation of Nuclear Emulsion Sensitized by Hydrogen Gas

H. Rokujo, Y. Isayama and T. Nakano
F-lab., Graduate School of Science, Nagoya University, Nagoya 464-8602, Japan

Nuclear emulsion is currently being used for particle and radiation measurements in a variety of scientific and applied fields. After its production, the nuclear emulsion records tracks of charged particles until it is developed. If the sensitivity can be controlled before and after experiments/observations, and if it can be given a switch function to turn them on and off, the use of nuclear emulsion is expected to expand into new applications. For example, this ON/OFF function would be an effective basic technology for transporting nuclear emulsion to space.

Hydrogen hyper-sensitization is known as one of the sensitization processes in astrophotography. The principle of this method is that the reducing action of hydrogen gas is used to produce reduction sensitization centers on silver bromide crystals, resulting in an increase in sensitivity [1]. By baking the film with hydrogen gas before exposure, the sensitivity can be temporarily increased. Conventional photographic film is used in air, so it retains its sensitivity for only a few days after gas treatment. There is no report on the combination of nuclear emulsion film and hydrogen hyper-sensitization that has been put into practice. We attempted to control the sensitivity of nuclear emulsion using hydrogen gas and evaluated the sensitivity by irradiating electrons obtained by UVSOR.

Nuclear emulsion plates were prepared by coating gold-sulfur sensitized and unsensitized nuclear emulsion gels (AgBrI crystals, average particle size 240 nm, gelatin volume ratio ~60 %) on glass slides, respectively. The plates were placed in a small stainless steel pressure vessel and the vacuum pump was used to reduce the gauge pressure to -95 kPa. Then, the vessel was filled with nitrogen gas and pressurized to a gauge pressure of +20 kPa. And hydrogen gas was filled to the gauge pressure of +25 kPa, so that the hydrogen gas content in the vessel was 4 %. The vessel was placed in a thermostatic bath and baked at 40 °C for 23 hours. After returning to room temperature for 1 hour, the vessel was opened, and the nuclear emulsion plate were extracted. The plates were immediately vacuum-sealed one by one, shut off from light/air, and stored frozen. Two days after the baking process, the plates were irradiated with electron beams at UVSOR and developed (XAA, 20 °C, 25 min) at Nagoya University on the day after irradiation.

Figure 1 shows a microscopic image of the electron beam tracks, and Fig. 2 shows the results of grain density measurements (average count of developing silver particles per 100 microns). The grain density did not increase in comparison with samples that were not gas-filled but were baked (40 °C for 23 hours) and refrigerated at the same time. No electron beam tracks were observed in the unsensitized emulsion sample.

Hydrogen hyper-sensitization test of nuclear emulsion was performed for the first time. Although no increase in sensitivity was observed, we were able to confirm the setup and procedures for processing and evaluation. In the future, we would like to change the baking conditions after sealing in nitrogen-hydrogen gas and find conditions to increase sensitivity.

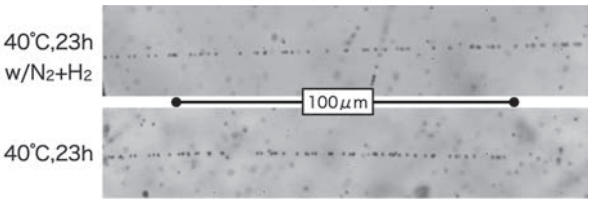

Fig. 1. Micrographs of electron tracks recorded in emulsion plates with and without hydrogen hyper-sensitization [2].

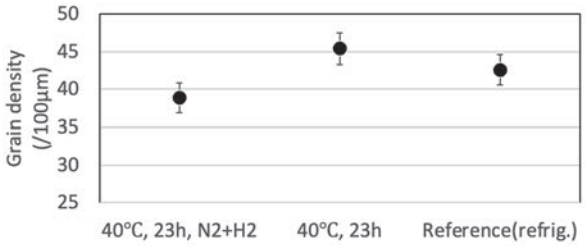

Fig. 2. Comparison of grain density between emulsion plates with and without hydrogen hyper-sensitization [2].

[1] T. Tani, J. Soc. Photogr. Sci. Tech. Jpn. **81** (2018) 108.
[2] H. Rokujo and Y. Isayama, J. Soc. Photogr. Sci. Tech. Jpn. **86** (2023) 426.

UVSOR User 3